Supplementary Information

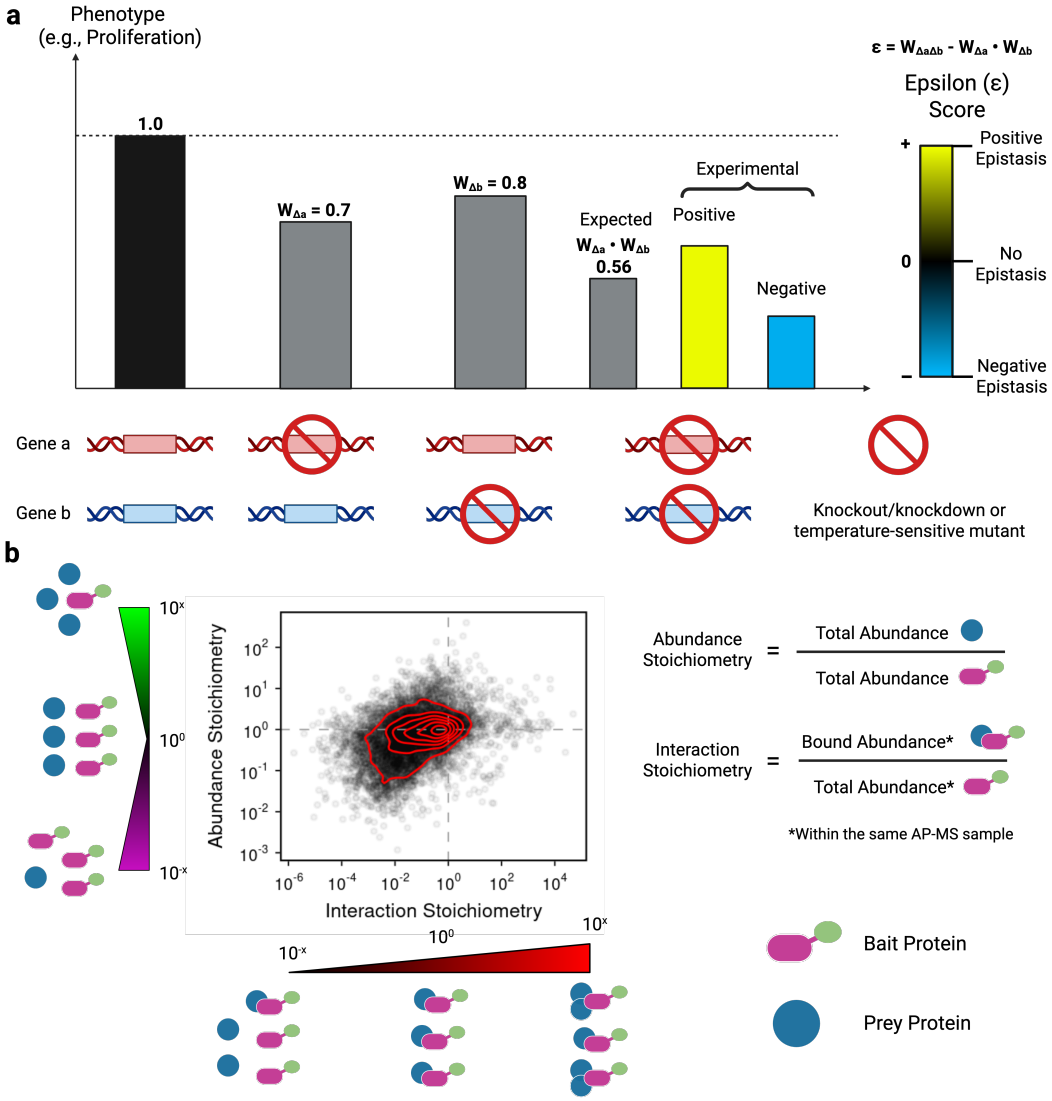

Supplementary Figure 1. Defining the quantitative features of the GI and PPI networks. a) Genetic interaction scores in yeast are calculated using the difference between expected double-knockout fitness (derived from a multiplicative model of single knockouts) and the actual experimental double-knockout fitness value. In human cell lines, the multiplicative model is replaced by a quadratic fit of single vs. double mutant fitness. Temperature-sensitive mutants are used instead of knockouts for essential genes in yeast, and CRISPR interference knockdown is used for all genes in mammalian cell lines. **b)** Illustrations and simplified formulas for the different stoichiometry measurements describing protein-protein interactions. Abundance stoichiometries are calculated by dividing the total abundance of the prey protein by that of the bait protein.

Interaction stoichiometries are calculated by dividing the number of bound bait-prey complexes by the total abundance of bait protein within the same AP-MS sample. Interaction stoichiometry and abundance stoichiometry data points are calculated from data generated in Michaelis et al.[1] The illustration was adapted from Hein et al.[2] using BioRender.

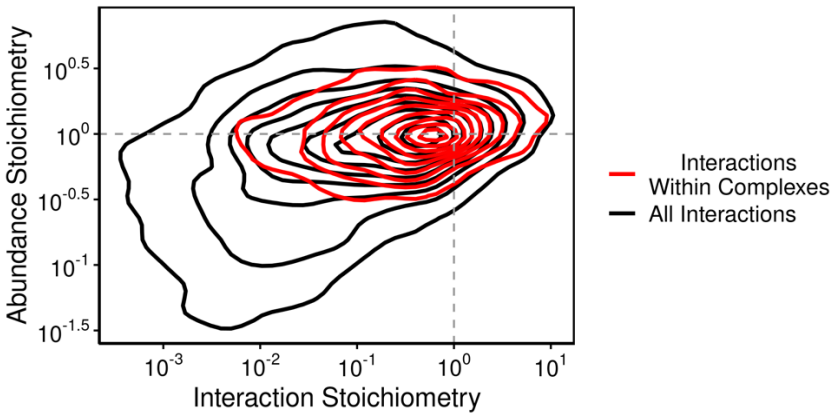

Supplementary Figure 2. Stable protein complexes in *Saccharomyces cerevisiae* are enriched for 1:1 stoichiometries. Yeast PPIs occurring between proteins of stable complexes as annotated by the ComplexPortal database[3]. Source data are provided as a Source Data file.

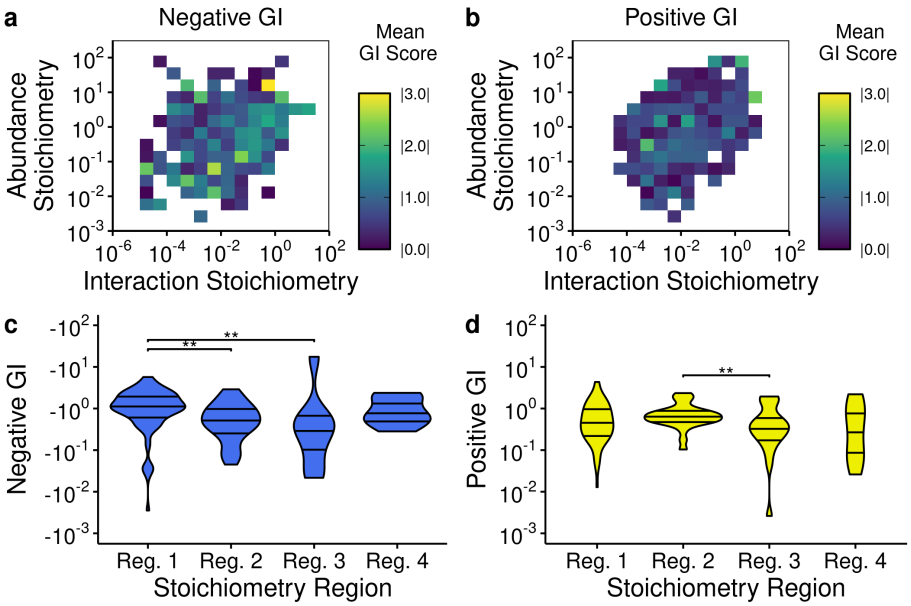

Supplementary Figure 3. The PPI stoichiometry landscape of GIs in the Jurkat cell line. a, b, Mean negative and positive genetic interaction scores for PPIs throughout the stoichiometry plot. GI scores in human were taken from a screen in Jurkat cell lines. **c, d,** Distribution of negative (c) and positive (d) GI scores within the 4 defined regions of the stoichiometry plot. Two-sided Wilcoxon rank-sum tests were used to assess differences. No correction for multiple comparisons was performed. Significance levels are annotated as: ** for $p \leq 0.01$. Source data are provided as a Source Data file.

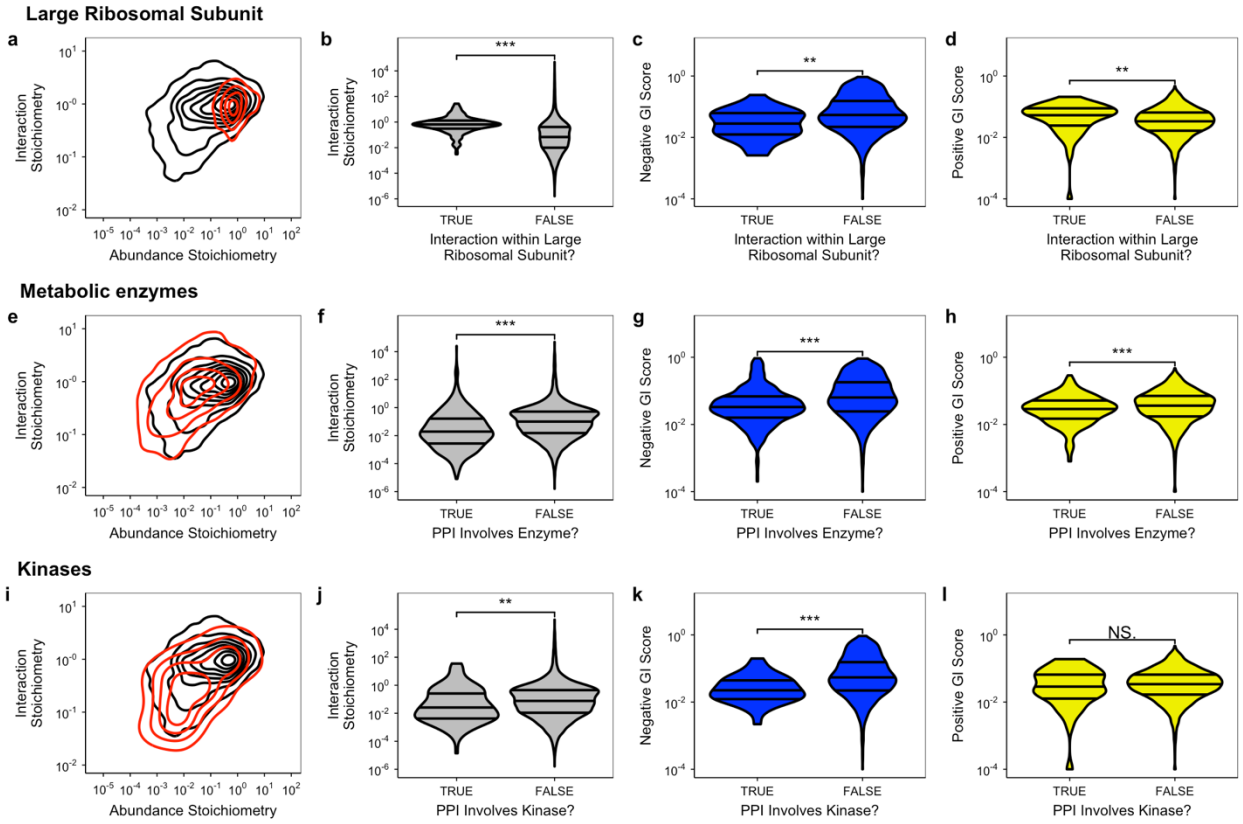

Supplementary Figure 4. Distribution of protein-protein interaction stoichiometries and genetic interactions across different functional gene/protein sets in yeast. a, e, i, Stoichiometry map of protein-protein interactions in which both proteins are subunits of the large ribosomal subunit (a), at least one protein involves a metabolic enzyme (e), and where a least one protein involves a kinase (i). Black contours represent the distribution of all PPIs, red contours represent interactions within the specific set of proteins. **b, f, j,** Distribution of interaction stoichiometries for large ribosomal subunits (b), metabolic enzymes (f), and kinases (j). **c, g, k,** Distribution of negative genetic interactions for large ribosomal subunits (c), metabolic enzymes (g), and kinases (k). Only pairs of genes that have both a GI score and form a PPI are considered. **d, h, l,** Distribution of positive genetic interactions for large ribosomal subunits (d), metabolic enzymes (h), and and kinases (l). Only pairs of genes that have both a GI score and form a PPI are considered. *p*-values are calculated using a two-tailed Wilcoxon rank sum test. Significance levels are annotated as: * for $p \leq 0.05$, ** for $p \leq 0.01$, and *** for $p \leq 0.001$, respectively. Source data are provided as a Source Data file.

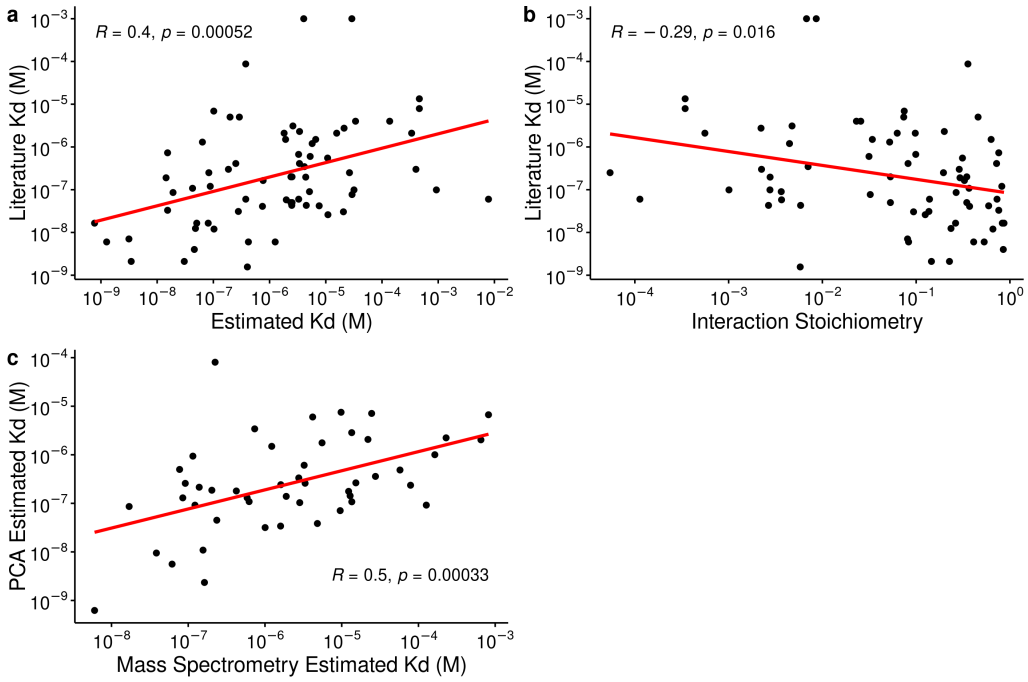

Supplementary Figure 5. Validation of dissociation constants estimated from quantitative mass spectrometry measurements. Pearson correlation was used in all panels, with two-sided tests for *p*-values. **a,** Estimated PPI dissociation constants estimated from quantitative mass spectrometry data in human cell lines correlate moderately but very significantly with values from literature. **b,** Interaction stoichiometries from quantitative mass spectrometry data in human cell lines correlate weakly with values from literature. **c,** Dissociation constants estimated from quantitative mass spectrometry data in yeast correlate moderately but very significantly with those estimated from protein-fragment complementation (PCA) results. Source data are provided as a Source Data file.

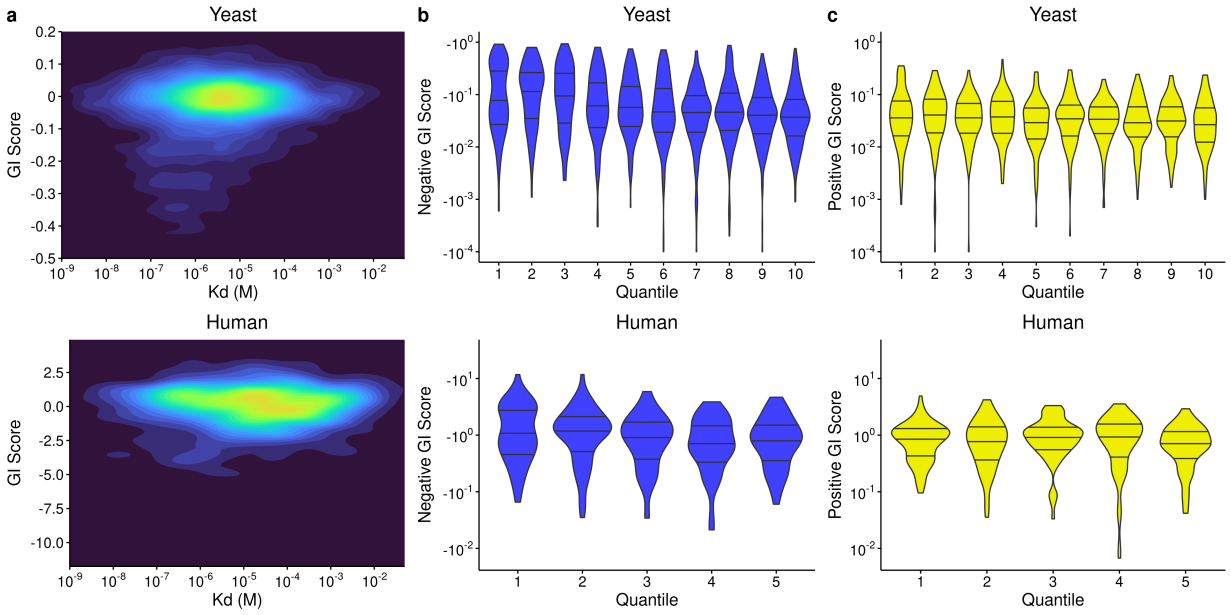

Supplementary Figure 6. High affinity protein-protein interactions are biased towards strong GIs. a, Density plot of genetic interaction scores as a function of their protein-protein interaction affinity (K_d) for yeast and human (K562 cell line). **b,** Distribution of negative GI scores across K_d quantiles (quantile 1 is the lowest K_d; strongest affinity) for yeast and human. **c,** Distribution of positive GI scores across K_d quantiles (quantile 1 is the lowest K_d) for yeast and human. Source data are provided as a Source Data file.

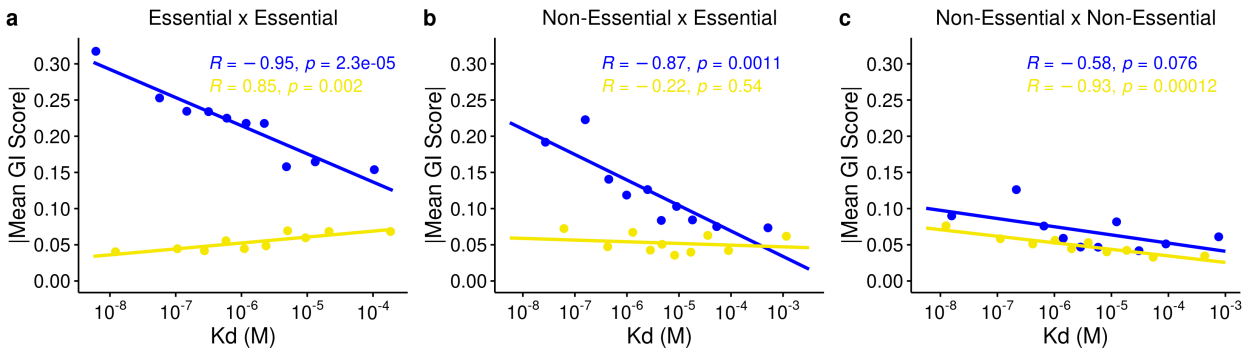

Supplementary Figure 7. Correlations between binned genetic interactions and K_d for genes pairs of different essentialities. a-c, Pearson correlation coefficients between dissociation constants (K_d) and GIs are computed for genes pairs where both genes are essential (a), only one gene is essential (b), or both genes are non-essential (c). *p*-values are computed from two tailed test. All trendlines are fit using a linear regression. Source data are provided as a Source Data file.

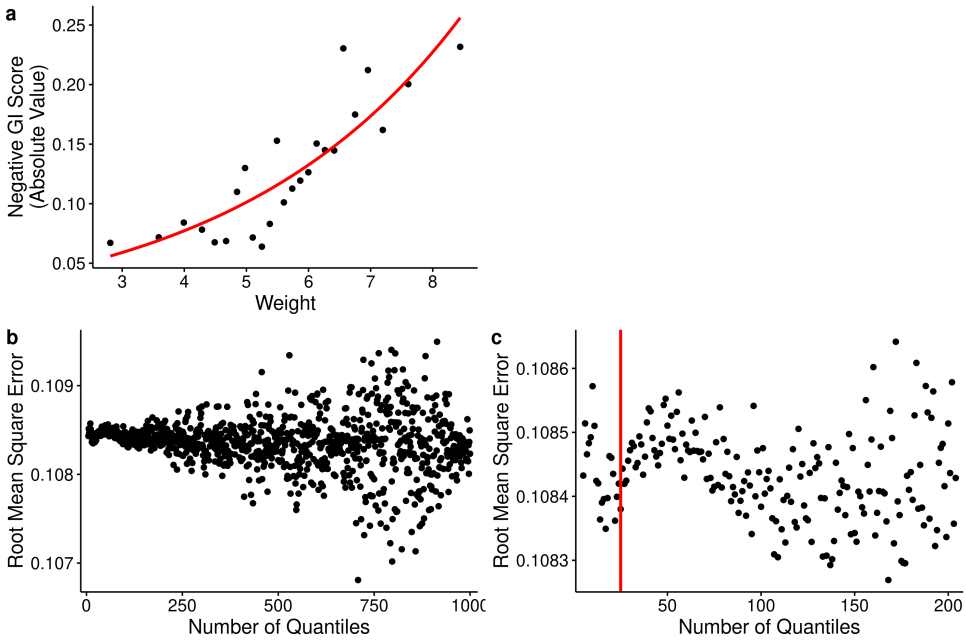

Supplementary Figure 8. Fitting an equation relating binned PPI weights (derived from K_d values) to GI scores. a, Yeast PPIs are binned into 25 quantiles according to their network weights. The average weight and GI score is calculated for every quantile and an exponential equation is used to fit the data. **b,** The fitting procedure described in (a) was tested with different numbers of quantiles to visualize their root mean square errors (RMSE). **c,** A narrowing of RMSE spread and a dip in RMSE values can be observed at around 25 quantiles. Source data are provided as a Source Data file.

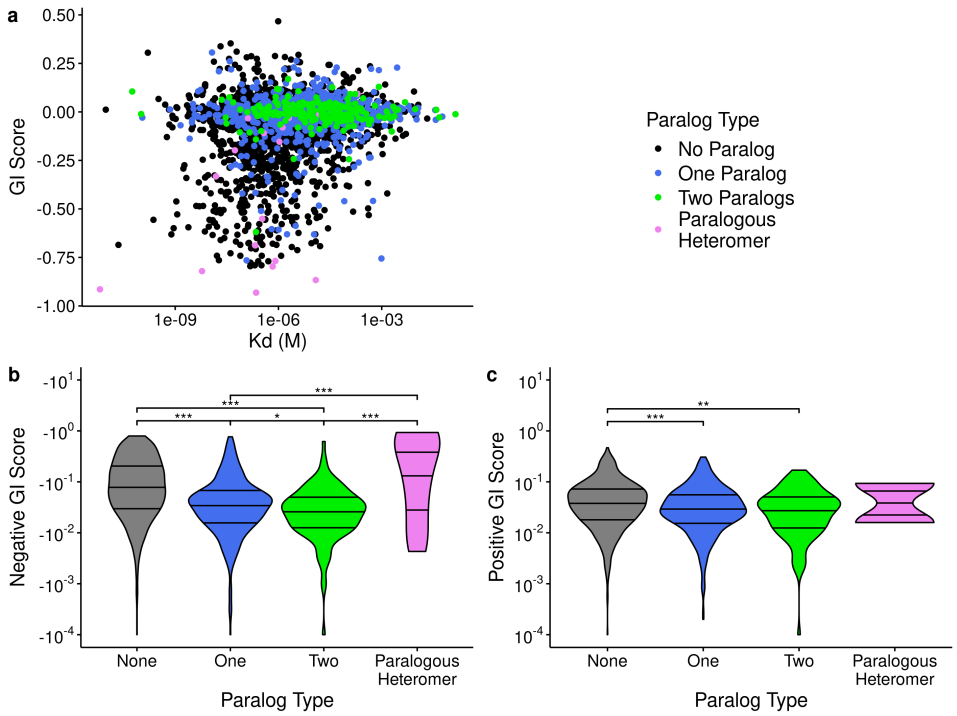

Supplementary Figure 9. Distribution of positive and negative genetic interaction scores according to PPIs separated by their paralog composition. a, Distribution of estimated K_d and GIs (yeast dataset) according to the PPI's paralog composition/type. **b,** Distribution of negative GI scores for different interaction type. **c,** Distribution of positive GI scores for different interaction type. Two-sided Wilcoxon rank-sum tests were used to assess differences. No correction for multiple comparisons was performed. Significance levels are annotated as: * for $p \leq 0.05$, ** for $p \leq 0.01$, and *** for $p \leq 0.001$, respectively. Source data are provided as a Source Data file.

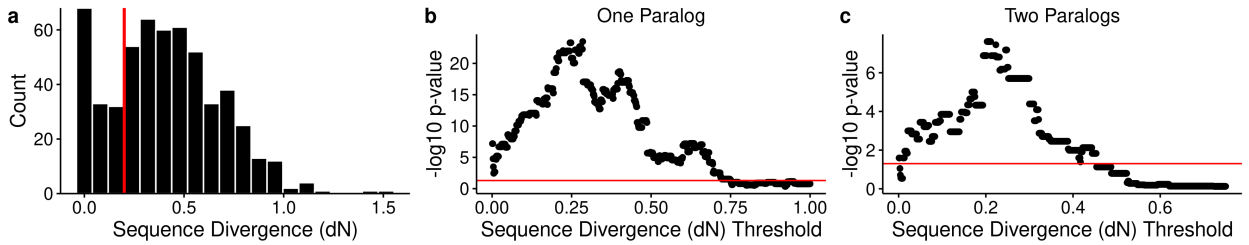

Supplementary Figure 10. Dividing protein-protein interactions according to paralog sequence divergence. a, Sequence divergence (dN) between paralogous protein/gene pairs retrieved from literature. A dN threshold of 0.2 separates the two visible modes in the distribution. **b, c,** The statistically significant differences in dissociation constants between high divergence and low divergence are robust to the chosen dN threshold. This holds for PPIs in which one protein has a paralog (b) and PPIs in which both proteins have a paralog (c). *p*-values are calculated using a two-sided Wilcoxon rank sum test, without multiple hypothesis correction. Red line indicates a *p*-value of 0.05. Source data are provided as a Source Data file.

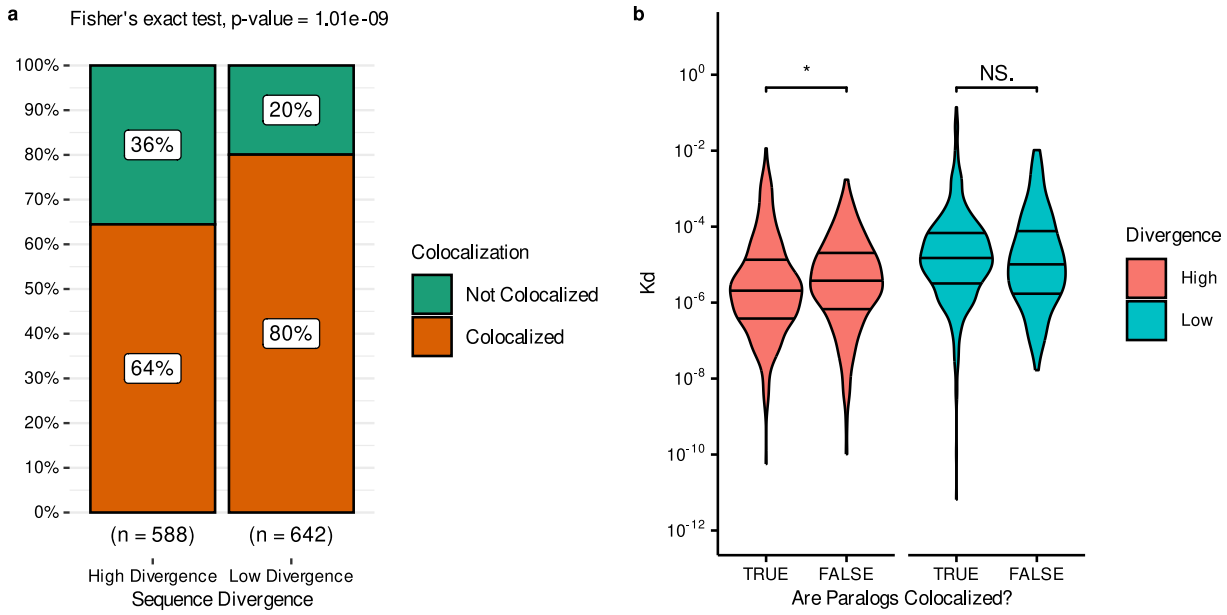

Supplementary Figure 11. Functional divergence is reflected in colocalization statistics, jointly with binding affinity. a, Functionally redundant paralogs (low sequence divergence) are more likely to colocalize than functionally divergent paralogs. A one-sided Fisher's exact test was used to calculate the p-value. **b,** Colocalization and functional divergence in paralogs are reflected in their affinities (K_d) with other proteins. For all panels, proteins are deemed to be "colocalized" if they share at least one localization alignment in the YeastGFP dataset[4]. *p*-values are calculated using a two-sided Wilcoxon rank sum test without correction for multiple hypothesis testing, significance levels are annotated as: * for $p \leq 0.05$ and NS. for $p > 0.05$ ("Not Significant"). Source data are provided as a Source Data file.

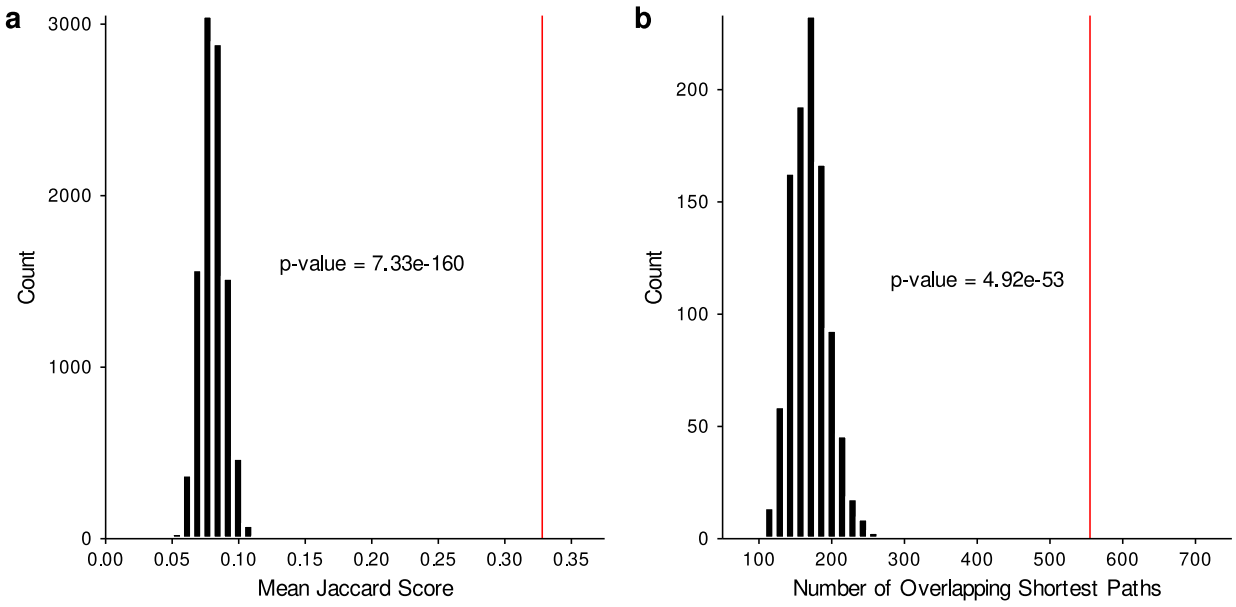

Supplementary Figure 12. The overlap of modules and shortest path connectors between GI and PPI networks is statistically significant. a, A statistical validation of overlaps between modules in GI and PPI networks by comparing the observed overlap with that of randomized modules. **b**, A statistical validation of overlaps between shortest path in GI and PPI networks by comparing the number of observed shortest path overlaps to that of randomized networks. One-sided *p*-values are calculated as probability of observing a z-score equal to or greater than that of the observed value (red), when compared to that of the randomized values (black). Source data are provided as a Source Data file.

Supplementary Table 1: Terminology and data related to results in figure 1

Term	Definition[a]	Organism	Data Source	Experimental approach
Interaction stoichiometry	Ratio of bound prey protein relative to bait protein abundance in an AP-MS sample	Yeast	Ref. 1[1,b]	Affinity-purification coupled to mass spectrometry
		Human	Ref. 2[2] Ref. 5[5]	
Abundance stoichiometry	Ratio of total abundances between two proteins	Yeast	Ref. 6[6,b]	GFP microscopy, GFP flow cytometry, mass spectrometry, TAP-Immunoblot
		Human	Ref. 2 Ref. 5[b]	Whole-cell mass spectrometry
Genetic interaction (epistasis)	Instances where the fitness of an experimental double genetic perturbation deviates from the value expected from single genetic perturbations	Yeast	Ref. 7[7]	Synthetic Genetic Array
		Human	Ref. 8[8]	CRISPR interference

[a]Operational definition used throughout this article.
[b]Data from the original source was further processed for the purpose of our analyses

Supplementary Table 2[a]: Essential Complexes Enriched for Negative GIs

ComplexPortal ID	Common Name
CPX-1890	Exocyst
CPX-1364	SMC5/6 complex
CPX-1041	DASH complex
CPX-1656	Transcription factor TFIIIC complex
CPX-607	Arp2/3 protein complex
CPX-1186	MIND complex
CPX-1869	Nuclear condensin complex
CPX-1831	Eukaryotic translation initiation factor 3 complex
CPX-2262	20S proteasome core particle
CPX-1895	mRNA cleavage factor complex

[a]Examples were taken from Costanzo et al. (2016)[7]

Supplementary Table 3[a]: Non-Essential Complexes Enriched for Positive GIs

ComplexPortal ID	Common Name
CPX-779	Elongator holoenzyme complex
CPX-1840	Golgi transport complex
CPX-568	CAF-1 complex
CPX-1197	FAR complex
CPX-1342	Set3C
CPX-1884	HDA complex
CPX-1193	Vacuolar proton-transporting V-type ATPase
CPX-1412	Ubp3-Bre5 ubiquitin hydrolase complex
CPX-1655	i-AAA complex
CPX-1178	Cytoplasmic dynein complex

[a]Examples were taken from Costanzo et al. (2016)[7]

Supplementary Table 4: Correlation coefficients between unbinned K_d and GI values

Organism	GI Type	Correlation Measure	Coefficient	p-value[a]
Yeast	Negative	Pearson	0.27	$< 2.2\times10^{-16}$
		Spearman	0.24	$< 2.2\times10^{-16}$
	Positive	Pearson	0.12	2.5×10^{-5}
		Spearman	0.092	1.0×10^{-3}
Human	Negative	Pearson	0.15	0.012
		Spearman	0.13	0.027
	Positive	Pearson	0.018	0.73
		Spearman	0.019	0.73

[a]All *p*-values are calculated using two-sided tests

Supplementary References

1. Michaelis, A. C. *et al.* The social and structural architecture of the yeast protein interactome. *Nature* **624**, 192–200 (2023).
2. Hein, M. Y. *et al.* A Human Interactome in Three Quantitative Dimensions Organized by Stoichiometries and Abundances. *Cell* **163**, 712–723 (2015).
3. Meldal, B. H. M. *et al.* Complex Portal 2018: extended content and enhanced visualization tools for macromolecular complexes. *Nucleic Acids Res* **47**, D550–D558 (2019).
4. Huh, W.-K. *et al.* Global analysis of protein localization in budding yeast. *Nature* **425**, 686–691 (2003).
5. Cho, N. H. *et al.* OpenCell: Endogenous tagging for the cartography of human cellular organization. *Science* **375**, eabi6983 (2022).
6. Ho, B., Baryshnikova, A. & Brown, G. W. Unification of Protein Abundance Datasets Yields a Quantitative Saccharomyces cerevisiae Proteome. *Cell Systems* **6**, 192-205.e3 (2018).
7. Costanzo, M. *et al.* A global genetic interaction network maps a wiring diagram of cellular function. *Science* **353**, aaf1420–aaf1420 (2016).
8. Horlbeck, M. A. *et al.* Mapping the Genetic Landscape of Human Cells. *Cell* **174**, 953-967.e22 (2018).